Ostwald ripening in two dimensions: Correlations and scaling beyond mean field

Boris Levitan and Eytan Domany
Department of Physics of Complex Systems, Weizmann Institute of Science, Rehovot, Israel
(Received 4 August 1997)

We present a systematic quasi-mean-field model of the Ostwald ripening process in two dimensions. Our approach yields a set of dynamic equations for the temporal evolution of the minority phase droplets' radii. The equations contain only pairwise interactions between the droplets; these interactions are evaluated in a mean-field-type manner. We proceed to solve numerically the dynamic equations for systems of tens of thousands of interacting droplets. The numerical results are compared with the experimental data obtained by Krichevsky and Stavans [Phys. Rev. Lett. **70**, 1473 (1993); Phys. Rev. E **52**, 1818 (1995)] for the relatively large volume fraction $\varphi = 0.13$. We found good agreement with experiment even for various correlation functions. [S1063-651X(98)04402-X]

PACS number(s): 64.60.My, 64.60.Cn, 64.75.+g

I. INTRODUCTION

When a system is quenched into a two-phase coexistence region, its homogeneous initial state no longer corresponds to thermodynamic equilibrium [1]. If there is a conserved quantity whose density is different in the two coexisting phases (such as the total volume or total amount of impurities), the final equilibrium state consists of two macroscopic domains, separated by a single phase boundary. The manner in which a system evolves from its homogeneous initial state to the final equilibrium state of two-phase coexistence has been the subject of numerous theoretical and experimental investigations.

For small initial supersaturation the system's evolution towards two-phase equilibrium starts by nucleation and growth of droplets (or small crystallites) of the minority phase. In the late stage of evolution to the equilibrium state no new droplets are formed and the amount of material in each of the phases remains fixed. Evolution proceeds by means of dissolution of small droplets and growth of the large ones, giving rise to reduction of the total (surface) energy of the system. The exchange of material is driven by diffusion; the concentration is higher near surfaces with high curvature and hence the diffusive flux is directed from the small droplets towards the larger ones. This coarsening process [2], called *Ostwald ripening*, in the course of which the number of droplets decreases while the average size of the remaining ones increases, is the subject of the present paper.

In what follows we describe a formalism that leads to an efficient numerical algorithm for Ostwald ripening in two dimensions. Our work was motivated by and our results are compared with recent experimental work on a two-dimensional film of liquid and crystalline succinonitrile in coexistence [3]. Therefore, we will refer to the minority phase as ''solid'' and to the matrix in which the droplets are embedded as ''liquid.''

Ostwald ripening belongs to a family of nonequilibrium phenomena that exhibit evolution to a *scaling state*. By a scaling state we mean that there is a single length scale in the system, which grows with time. For Ostwald ripening the obvious length scale is the average droplet size $\langle R \rangle$; its growth with time follows the celebrated [4] Lifshitz-Slyozov law $\langle R \rangle \sim t^{1/3}$. When rescaled by this changing length, all statistical characteristics of the system (such as droplet size distribution and spatial correlations) are time independent. That is, by comparing two photographs of the system, taken at different (well separated) times but properly rescaled, one cannot tell from any statistical measurement which photograph was taken earlier.

A parameter of central importance on which various characteristics of the system (such as the droplet size distribution) depend is the relative volume fraction of the minority phase φ. This parameter determines the ratio of the size of the droplets and the distance between them. Therefore, φ controls the extent to which droplets interact with each other; for very small volume fractions the interaction is weak and any particular droplet ''feels'' the effect of the others only through an effective medium. This observation served as the basis of the theoretical, mean-field models [5–7] (see Ref. [8] for a review). As φ increases correlations between neighboring droplets become more important, until mean-field-based approximations lose their validity. The effects of correlations have been taken into account analytically to first order in a small parameter [9,10]. In three dimensions the small parameter is $\sqrt{\varphi}$ (see [9]) and in two dimensions it is $1/\ln\varphi$ (see [10]). The expressions obtained are so complicated even in first order that it is hard to see how one can proceed to higher orders. Rather, a combined analytical and numerical approach seems to be suitable.

The basic phenomenological description of Ostwald ripening is provided in the framework of a Cahn-Hilliard equation [11] (see Ref. [12] for a review) for the order parameter. Rogers and Desai [13] performed such a ''first-principles'' computation, reaching the scaling state with about 500 droplets. This was achieved for small values of φ (less than 0.1), when all the droplets were almost circular. Such a number of droplets suffices for studying the droplet size distribution, but is too small to gain insight into the spatial and temporal correlations in the scaling state. Moreover, for larger fractions the final stage of the coarsening process was not achieved in the calculation and scaling was not observed. Masbaum [14] used this method recently for a simulation, performed on a parallel computer, starting with about 3000 droplets. He obtained rather good agreement for various cor-

relation functions with the experiments of Krichevsky and Stavans [3].

It is clear, however, that this method can hardly be applied for studying much larger systems, which are needed in order to make statistically meaningful measurements in the late-stage scaling regime. Therefore, one turns to simplified descriptions of the system, hoping that the main features of the full Cahn-Hilliard theory are preserved. For the sake of completeness, we briefly present below a sequence of approximations that lead from the full Cahn-Hilliard theory to our approach.

First, one goes to a coarse-grained representation of the order-parameter field, which retains the *boundaries* between the crystalline droplets and the surrounding liquid as one of the dynamic variables of the problem. The second variable is the diffusing *concentration field* (of the impurities or the liquid itself) $c(\vec{r})$. Simplification of the problem is attained by separation of time scales. The process that occurs on fastest scales is the equilibration of the concentration near the (moving) boundaries. Assuming that this occurs instantaneously allows us to write the Gibbs-Thomson condition for the concentration at a point on the boundary of a droplet, where the (local) radius of curvature is $R(t)$:

$$c|_{droplet}(t)=c_{eq}(R(t))=c_\infty+\frac{\alpha}{R(t)}. \tag{1}$$

Here c_∞ is the equilibrium concentration in a liquid above a *planar* liquid-solid interface. The problem becomes now one of solving the diffusion equation

$$\frac{\partial c}{\partial t}=\nabla^2 c \tag{2}$$

with boundary conditions given by Eq. (1) on *moving boundaries*.

The rate of change of the boundaries is determined by $J_\perp=\hat{n}\cdot\vec{J}$, the mass flux normal to the droplet's surface, which in turn is proportional to the gradient of the concentration field at the boundary:

$$\frac{dR}{dt}=-J_\perp, \quad \vec{J}=-\vec{\nabla}c|_R. \tag{3}$$

Equations (1)–(3) constitute a closed dynamical problem. The next simplification is a quasistatic approximation to the problem. For *fixed* boundary conditions the diffusing field would reach a steady state in a characteristic diffusion time $t_D\sim R^2$, where R is a typical length scale (distance between neighboring droplets). If this time is much shorter than the growth time t_G, i.e., the time it takes a typical droplet's radius to change appreciably, the concentration field reaches a steady state before the radii of the droplets had a chance to change and one can use the stationary diffusion equation instead of Eq. (2). This is precisely the case for late stages of the growth process, where $t_G\sim R^3$, so that indeed $t_D\ll t_G$. The Lifshitz-Slyozov scaling law $t_G\sim R^3$ can be established by dimensional analysis of Eqs. (1) and (3). Hence, at late stages the solution $c(\vec{r},t)$ of Eq. (2) can be approximated by the solution of the stationary diffusion problem

$$\nabla^2 c=0 \tag{4}$$

with the previous boundary conditions (1); however, now we look for a solution of Eq. (4), from which the rate of change of the boundaries is obtained using Eq. (3), giving rise to new boundaries at the next time step and so on. It should be noted that in this approximation the total area of the droplets is conserved exactly.

It is possible to reformulate the stationary diffusion problem (1)–(4) as an integral equation that automatically accounts for the boundary conditions. Expanding the shapes of the droplets using a set of orthogonal polynomials, one can reduce the problem to an *implicit* system of ordinary differential equations in terms of the expansion coefficients [15–17].

Further simplification can be achieved by neglecting the deviation of the droplet shapes from circular. We expect this approximation to work for low volume fractions φ, when the distances between the droplets are much larger than the droplets sizes and redistribution of material in a single droplet is much faster than the exchange between the well-separated droplets. However, experiments [3] show that even for fractions as large as $\varphi=0.4$ the droplets are more or less circular. Therefore, we consider Laplace's equation (4) with the boundary conditions (1) at perfectly circular domains of radii R_i, positioned at points $\vec{r}_i$. This is a problem in electrostatics: calculating the potential in the presence of conducting cylinders. One approximates the solution of this problem by

$$c(r)=\sum_i q_i\ln(|\vec{r}-\vec{r}_i|/R_0)+\sum_i \frac{\vec{p}_i\cdot(\vec{r}-\vec{r}_i)}{|\vec{r}-\vec{r}_i|^2}, \tag{5}$$

where R_0 is an arbitrary length. The ''charges'' q_i and the ''dipoles'' p_i should be chosen so that the boundary conditions (1) are satisfied (approximately) on the surface of each droplet. Let us denote by $X_{ij}=|\vec{r}_i-\vec{r}_j|$ the distance between the centers of droplets i and j and by $c|_{R_i}$ the correct boundary value of the concentration, as given by Eq. (1). We now approximate the concentration field at the the boundaries by its expansion to first order in the small parameter R_i/X_{ij}:

$$c_\infty+\frac{\alpha}{R_i}=c(\vec{r}_i+\vec{R}_i)\approx q_i\ln R_i/R_0+\frac{\vec{p}_i\cdot\vec{R}_i}{R_i^2}+\sum_{j\neq i} q_j\ln(X_{ij}/R_0)+\sum_{j\neq i}\frac{\vec{p}_j\cdot\vec{X}_{ij}}{|X_{i,j}|^2}+\sum_{j\neq i} q_j\frac{\vec{X}_{i,j}\cdot\vec{R}_i}{|X_{i,j}|^2}. \tag{6}$$

$\vec{R}_i$ denotes the radius vector of points on the surface of droplet i; the last term appears as the expansion of $q_j\ln|\vec{r}_i+\vec{R}_i-\vec{r}_j|$. Equation (6) contains two parts: one that depends on the direction of $\vec{R}_i$ and one that does not. This results in two sets of linear equations for the charges and the dipoles:

$$c_\infty+\frac{\alpha}{R_i}=q_i\ln R_i/R_0+\sum_{j\neq i} q_j\ln(X_{ij}/R_0)+\sum_{j\neq i}\frac{\vec{p}_j\cdot\vec{X}_{ij}}{|X_{i,j}|^2}, \tag{7}$$

$$\frac{\vec{p}_i\cdot\vec{R}_i}{R_i^2}+\sum_{j\neq i} q_j\frac{\vec{X}_{i,j}\cdot\vec{R}_i}{|X_{i,j}|^2}=0. \tag{8}$$

As we will see, the last term in Eq. (7) is $O((R/X)^2)$, i.e., smaller than the other terms, and can be omitted. Thus the system of equations

$$c_\infty+\frac{\alpha}{R_i}=q_i\ln R_i/R_0+\sum_{j\neq i} q_j\ln(X_{ij}/R_0) \tag{9}$$

determines the charges. Since Eq. (8) should be satisfied for any $\vec{R}_i$, the dipoles are determined by

$$\frac{\vec{p}_i}{R_i^2}=-\sum_{j\neq i} q_j\frac{\vec{X}_{i,j}}{|X_{i,j}|^2}. \tag{10}$$

The physical meaning of Eq. (10) is that the dipole associated with droplet i is simply related to the electric field induced at its center by all the other charges. Once the charges are obtained from solving Eq. (9), their substitution in Eq. (10) determines the dipoles.

The normal component of the flux at the boundary of droplet i is given by

$$\nabla_n c(\vec{r}_i+\vec{R}_i)=\frac{q_i}{R_i}-2\frac{\vec{p}_i\cdot\vec{R}_i}{R_i^3}, \tag{11}$$

where Eqs. (6) and (10) were used. The normal flux has two contributions: an isotropic part, giving rise to a rate of change of the radius, given by

$$\frac{dR_i}{dt}=\frac{q_i}{R_i}, \tag{12}$$

and an anisotropic part, due to the dipole term in Eq. (11). The contribution of the dipole part to the *total* flux vanishes; it induces deposition of material on one side of the droplet and evaporation from the opposite side. We approximate the effect of the dipole flux by *shifting the positions* of the circular droplets (see below). We also show (in Appendix A) that in the low concentration ($\varphi\ll 1$) limit the effect of the dipoles is negligible; we discuss this limit first, working with charges only, and then include the dipoles.

Equation (12) implies that the rate of change of the area of droplet i is proportional to its charge q_i. Using q_i from Eq. (12) in Eq. (9) eliminates the concentration field $c(\vec{r})$ from the problem and, after proper rescaling of variables, the following set of equations for the temporal evolution of the radii results:

$$(1+R_i/R_c)=\sum_j L_{i,j}\dot{R}_j, \tag{13}$$

where $R_c=\alpha/c_\infty$ is a capillary length and the matrix $L_{i,j}$ defined in two dimensions (2D) as [15]

$$L_{i,j}=R_iR_j\times\begin{cases}\ln(R_i/R_0) & \text{if } i=j\\ \ln(X_{i,j}/R_0) & \text{otherwise.}\end{cases} \tag{14}$$

Clearly, solving the system of equations (13) and (14) is a much simpler computational task than solving the Laplace problem (4) with moving boundary conditions on the surfaces of the droplets. Note, however, that the matrix elements $L_{i,j}$ grow with the distance between the droplets. Because of this, finite-size effects become crucial: All droplets in the bulk feel the boundary. The simplest way to avoid this problem is to consider the system with periodic boundary conditions; the interaction of a pair of droplets contains an infinite sum of logarithms, corresponding to all the *images* of these droplets. Yao *et al.* [18] have summed this series using Ewald summation techniques.

The problem is further complicated by the need to invert the $N\times N$ matrix $L_{i,j}$ at *each* time step in order to get from Eq. (13) *explicit* expressions for $\dot{R}_i$. Thus, solving the system of equations (13) and (14) takes N^3 operations per time step; therefore, each run costs N^4 operations. This necessitates huge CPU times (the simulations of Yao *et al.* [18] took about 1000 CPU h on an IBM 3090 computer for a system of about 3000 droplets).

Beenakker [19] has solved an analogous problem in 3D by truncating the matrix $L_{i,j}$ [defined in 3D in a way analogous to Eq. (14)]. He took into account only the interactions between droplets whose separation does not exceed a threshold, reducing in this way the number of droplets with which a given one interacts to about 20. The physical motivation for such truncation is *screening* [20,21]; droplets whose separation exceeds the screening length do not affect each other. It should be noted that with such a truncation the total volume of the droplets is not conserved and Beenakker had to adjust R_c in Eq. (14) at each time step in order to restore volume conservation.

Akaiwa and Meiron [17] used the analogous truncation procedure in 2D. Although the interactions between the charges are expected to be well screened even in 2D, formal truncation of the matrix seems problematic in this case. Since the matrix elements grow with distance between the droplets, the elements of the *inverse* matrix as functions of the cutoff should contain large fast oscillating components (unlike in 3D, where their dependence on the cutoff is smooth). Nevertheless, their results (in particular, the correlation functions) compare well with experiment. Apparently, this success is due to the fact that these oscillations are effectively averaged out during the run.

Our goal was to find an analytic way of approximating $\hat{L}^{-1}$ in a manner that reflects screening as the physical basis of the approximation scheme. Once L has been inverted, we can integrate the equation

$$\dot{R}_i=\sum_j L^{-1}_{i,j}(1+R_j/R_c) \tag{15}$$

numerically. The approximation introduced in this work can be summarized by the expression

$$\dot{R}_i=\sum_j L^{-1}_{i,j}=\frac{1}{R_iK_0(R_i/\zeta_{sc})_j}\sum_{(\neq i)}\frac{K_0(X_{i,j}/\zeta_{sc})}{K_0(R_j/\zeta_{sc})}\left(\frac{1}{R_j}-\frac{1}{R_i}\right), \tag{16}$$

where K_0 is the zeroth-order modified Bessel function of the second kind (also called the MacDonald function). Since

TABLE I. Various quantities related to the self-consistent determination of $\phi(r)$ (with the depletion zones taken into account) for different area fraction φ. R_0 and ζ_0 are (simultaneous) solutions of Eqs. (B19), (B21) (with $d=2.15\langle R\rangle$ in both), and (B25); ζ_{mf} is the value of the screening length as obtained in Sec. III (neglecting the effect of the depletion zones); ζ_{scr} is determined by Eq. (B26) with $\phi(r)$ obtained by numerical integration. All lengths are given in units of $\langle R\rangle$.

φ	R_0	ζ_0^{mf}	ζ_0	ζ_{scr}
0.001	51.35	45.99	45.96	45.922
0.01	15.59	11.77	12.13	11.71
0.05	8.10	4.08	4.73	4.00
0.13	6.14	1.88	2.73	1.94

$K_0(x)\sim\exp(-x)$ for large x, the parameter ζ_{sc} has the meaning of a screening length. In the mean-field limit (i.e., for very small area fraction φ) it is determined by the equation

$$\zeta_{sc}^{-2}=2\pi n\left\langle\frac{1}{K_0(R/\zeta_{sc})}\right\rangle. \tag{17}$$

However, for larger fractions, where the effects of correlations become important, ζ_{sc} is determined by a more complicated condition, as discussed in Appendix B. In practice, in our simulations for $\varphi=0.13$ we used $\zeta_{sc}=2.73\overline{R}$, as determined by Table I (see Appendix B for details).

In spite of various approximations that were made to derive Eqs. (16) and (17), we believe that they contain the most important aspects of the dynamics present in Eq. (13). One can see explicitly the effects of screening, with the screening length appearing naturally in the derivation presented below. The total area is conserved explicitly. In the limit of very small minority phase area fractions, where $\langle R\rangle/\zeta_{sc}\to 0$, our description is consistent with Marqusee's mean-field theory [7], which leads to the following dynamical equation for the droplet's radius:

$$R\frac{dR}{dt}=k(R/\zeta)\left(\frac{1}{R}-\frac{1}{R_c}\right), \tag{18}$$

where $k(x)=xK_1(x)/K_0(x)$, while ζ is defined by the equation $\zeta^{-2}=2\pi n\langle k(R/\zeta)\rangle$. Since $xK_1(x)\to 1$ for $x\to 0$, we find $k(x)\to 1/K_0(x)$ and our definition of the screening length coincides with his. We used the formalism presented above to integrate the evolution of large assemblies of droplets and found that at relatively large values of the area fraction φ the droplets' motion, induced by the so far neglected dipoles, becomes important and must be taken into account.

We evaluate now the contribution of the dipoles to the shift of the droplets' centers of mass $\delta\vec{r}_i$, defined by

$$M\,\delta\vec{r}=\int\vec{R}\;\delta m. \tag{19}$$

Here the integration is over the boundary of a droplet; $\vec{R}$ is a radius vector on its boundary, $M=\rho\pi R^2$ is the total mass of the droplet (ρ is the density; it will drop out of the final result), and δm is the additional mass adsorbed (or lost) locally, due to the shift of the boundary during the interval dt. The anisotropic component of the local velocity of the droplet's boundary is given by

$$v=-J_n=-\frac{2p\cos\theta}{R^2},$$

where θ is the polar angle between $\vec{R}$ and $\vec{p}$. The mass added at $\vec{R}$ is

$$\delta m=\rho(v\;dt)(R\;d\theta)=-(2p/R)\rho\;dt\;\cos\theta\;d\theta,$$

so that (see also Appendix A of [9])

$$\frac{d\vec{r}}{dt}=-\frac{2p}{\pi R^3}\int\vec{R}\cos\theta\;d\theta=-\frac{2\vec{p}}{\pi R^2}\int\cos^2\theta\;d\theta=-\frac{2\vec{p}}{R^2}.$$

Finally,

$$\frac{d\vec{r}_i}{dt}=-\frac{2\vec{p}_i}{R_i^2}=2\sum_{j\neq i}\frac{q_j}{|X_{i,j}|}\frac{\vec{X}_{i,j}}{|X_{i,j}|}. \tag{20}$$

Note that both sides of Eq. (20) have the same dimensionality since the charges q_i are measured in area per time [see Eq. (12)].

The procedure for solving Eqs. (13) and (14) for the dynamics of the droplets' radii R_i, together with Eq. (20) for their positions $\vec{r}_i$, is as follows. For given $\vec{r}_i$ and R_i we invert $\hat{L}$, obtain dR_i/dt [or q_i as given by Eq. (12)], and integrate one time step. Next, substituting q_i into Eq. (20), we obtain new values of $\vec{r}_i$ and the procedure is repeated.

The sum on the right-hand side of Eq. (20) appears to be problematic: Assuming that the droplets' charges are uncorrelated (while the total charge is zero), one can see that the mean square of this sum diverges logarithmically with the size of the system. However, as we show in Appendix A, the correlations between the charges, provided by screening, ensure the convergence of this sum, so that it can be evaluated using a reasonable fraction of its terms. Actually, a *heuristic* formula, simpler than Eq. (20), can be used to evaluate the droplets' shifts in practical simulations. As explained in Appendix A, Eq. (20) can be replaced by

$$\frac{d\vec{r}_i}{dt}=2\sum_{j\neq i}\frac{K_{j,i}}{k_ik_j}\left(\frac{1}{R_i}-\frac{1}{R_j}\right)\frac{\vec{X}_{i,j}}{|X_{i,j}|^2}, \tag{21}$$

where $K_{i,j}=K_0(X_{i,j}/\zeta_{sc})$ and $k_i=K_0(R_i/\zeta_{sc})$. Although the approximation leading to this formula is not clearly established, our simulations show that it works as well as the more rigorous equation (20). At the same time it is much more economic because only droplets that lie within the screening length (from the droplet whose shift is evaluated) contribute to the sum.

In the sequence of approaches to the Ostwald ripening problem in two dimensions, ranging from the Cahn-Hilliard equation to Marqusee's mean-field theory, our model, which includes only the pairwise interaction between the droplets, can be viewed as the *minimal extension* of the mean-field approach. This concerns our Eq. (21) [in comparison with

Eq. (20)] as well. We believe that our approach constitutes the simplest step that can be taken beyond simple mean field.

Our program is as follows. In the next section we present a few universal properties of the matrix L. This is followed by Sec. III, where we derive the main result [Eq. (16)] using a mean-field-type approximation to L^{-1}. Numerical solutions of the resulting dynamics, based on Eq. (16) and Eq. (20) or (21), are presented in Sec. IV and compared with experiments by Stavans and Krichevsky. Section V presents a short summary of our approach and results.

II. SUM RULES

We present now some important properties of the matrix L^{-1} that lead to useful ''sum rules.'' The first claim is that

$$\sum_i L^{-1}_{i,j} R_i = \sum_j L^{-1}_{i,j} R_j \to 0 , \tag{22}$$

the sum approaching zero as the system size increases. This relationship is analogous to one presented for the three-dimensional case by Beenakker and Ross [22]. We present here arguments (which seem to us simpler than those of Ref. [22]) for the validity of Eq. (22) in 2D. First consider the quantity

$$a_j = \sum_i L_{i,j}/R_j = \sum_i R_i \ln(X_{i,j}/R_0). \tag{23}$$

The sum is clearly dominated by regions that are far from $\vec{r}_j$; in the absence of long-range correlations the composition of such regions does not depend on the identity of droplet j. On the other hand, the contribution of those droplets i that lie near droplet j *will*, in general, depend on R_j. By ''near'' we mean the region for which correlations *are* important. The size of this region is, however, small (on the order of the screening area; see below), the values of X_{ij} in this region are small, and the contribution from it is negligible compared to those from the far-away parts of the plane. That is, for increasing system size $a_j \to \infty$, whereas the contribution from the correlation region remains finite. Hence we can write

$$a_j = \sum_i L_{i,j}/R_j \simeq a \to \infty. \tag{24}$$

Next, consider the sum

$$1 = \sum_k \delta_{ik} = \sum_k \sum_j L^{-1}_{i,j} L_{j,k} = \sum_j L^{-1}_{i,j} R_j \sum_k L_{j,k}/R_j$$

$$= \sum_j L^{-1}_{i,j} R_j a_j . \tag{25}$$

Using now Eq. (24), we get

$$a \sum_j L^{-1}_{i,j} R_j \simeq 1, \tag{26}$$

so that

$$\sum_j L^{-1}_{i,j} R_j \simeq a^{-1} \to 0 \tag{27}$$

and hence statement (22) holds in the limit of large system size. An immediate consequence of Eq. (27) is obtained by using it in Eq. (15), yielding

$$\dot{R}_i = \sum_j L^{-1}_{i,j} . \tag{28}$$

Thus we see that the length R_c drops out from the description of the dynamics of the system.

Multiplying by R_i, summing over i, and using again Eq. (27), we establish area conservation

$$\sum_i R_i \dot{R}_i = \sum_j \left(\sum_i L^{-1}_{i,j} R_i \right) = 0 \tag{29}$$

as a consequence of our sum rule. Another important consequence is the following observation: L^{-1}_{ij}, the elements of the inverse matrix, are *independent of the parameter* R_0. To see this, take the derivative of $(L^{-1}L)_{i,k}$ with respect to $\ln R_0$: Clearly, $(L^{-1})' L + L^{-1} L' = 0$ and hence

$$(L^{-1}_{i,m})' = -\sum_{j,k} L^{-1}_{ij} L'_{jk} L^{-1}_{km} . \tag{30}$$

However, from Eq. (14) we immediately get that $(L_{j,k})' = -R_j R_k$, which when used in Eq. (30) gives

$$(L^{-1}_{i,m})' = -\sum_j \sum_k (L^{-1}_{k,m})' R_k L^{-1}_{i,j} R_j , \tag{31}$$

and when Eq. (27) is used here we get

$$(L^{-1}_{i,m})' = 0 \tag{32}$$

and hence L^{-1}_{ij} does not depend on R_0; in view of Eq. (28) the system's dynamics is therefore also independent of R_0.

III. MEAN-FIELD APPROXIMATION TO L^{-1}

Let us decompose the matrix $\hat{L}$ of Eq. (14) to its diagonal and off-diagonal parts

$$\hat{L} = \hat{L}_0 - \hat{L}_1 , \tag{33}$$

where $(\hat{L}_0)_{i,j} = \delta_{i,j} R_i^2 \ln(R_i/R_0)$ and $(\hat{L}_1)_{i,j} = -R_i R_j \ln(X_{i,j}/R_0)$. Note that only the off-diagonal part contains interactions between different droplets. One could consider an expansion of $\hat{L}^{-1}$ in powers of the interaction

$$\hat{L}^{-1} = (1 - \hat{L}_0^{-1}\hat{L}_1)^{-1} \hat{L}_0^{-1} = \sum_{n=0}^{\infty} (\hat{L}_0^{-1}\hat{L}_1)^n \hat{L}_0^{-1}, \tag{34}$$

with $\hat{L}_0^{-1}$ given by

$$(\hat{L}_0^{-1})_{i,j} = \delta_{i,j} \frac{1}{R_i^2 \ln(R_i/R_0)} . \tag{35}$$

Clearly, for matrix elements that correspond to well-separated droplets (i.e., when $X_{ij} \gg R_0$), terms of order $n+1$ will be larger than those of order n: that is, the series diverges formally and in order to obtain meaningful results one should perform some kind of partial summation to all orders. To do this we introduce the *T matrix*, defined by

$$\hat{L}^{-1} = \hat{L}_0^{-1} + \hat{L}_0^{-1} \hat{T} \hat{L}_0^{-1}. \tag{36}$$

To ensure that $\Sigma_j L_{i,j} L_{j,k}^{-1} = \delta_{i,k}$, $\hat{T}$ has to satisfy the equation

$$\hat{T} = \hat{L}_1 + \hat{L}_1 \hat{L}_0^{-1} \hat{T}. \tag{37}$$

For the sake of convenience we introduce a new matrix $\hat{\phi}$, defined by

$$T_{i,j} = R_i R_j \phi_{i,j}. \tag{38}$$

Once the matrix $\phi_{i,j}$ has been found, it is straightforward to write down $\hat{T}$ and, using Eq. (36), the inverse matrix $\hat{L}^{-1}$. Rewriting Eq. (37) in terms of $\hat{\phi}$, we get

$$\sum_{j\,(\neq i)} \frac{1}{\ln(R_j/R_0)} \ln(X_{i,j}/R_0)\, \phi_{j,k} + \phi_{i,k} = -(1-\delta_{ik}) \ln(X_{i,k}/R_0). \tag{39}$$

For the diagonal elements this takes the form

$$\phi_{k,k} = -\sum_{j \neq k} \frac{1}{\ln R_j/R_0} \ln(X_{k,j}/R_0)\, \phi_{j,k}, \tag{40}$$

whereas for the off-diagonal elements we obtain from Eq. (39)

$$\sum_{j \neq i,k} \frac{1}{\ln R_j/R_0} \ln(X_{i,j}/R_0)\, \phi_{j,k} + \phi_{i,k} = -\gamma_k \ln X_{i,k}/R_0, \tag{41}$$

where

$$\gamma_k = 1 + \frac{\phi_{k,k}}{\ln(R_k/R_0)}. \tag{42}$$

It should be noted that Eqs. (40)–(42) are exact. In principle, for any configuration of droplets, the set of equations (39) are to be solved for the matrix elements $\phi_{i,k}$. We approximate the solution of this problem in a *mean-field* spirit. The central premise of this mean-field approach is that the off-diagonal matrix elements $\phi_{i,j}$ depend only on the distance $X_{i,j}$, i.e.,

$$\phi_{i,j} = \phi(|\vec{r}_i - \vec{r}_j|). \tag{43}$$

That is, we are interested only in the *pairwise* interaction between the droplets (neglecting any possible dependence of $\phi_{i,j}$ on other droplets). The analogous approximation for the diagonal elements is that they are all equal, i.e. $\phi_{k,k}^{mf}$ is independent of k,

$$\phi_{k,k} \approx \phi_{k,k}^{mf} = \phi_0. \tag{44}$$

To obtain manageable mean-field equations the following simplifying assumptions are made: (i) In sums such as Eqs. (40) and (41) replace $1/\ln(R_j/R_0)$ by its average value [23], (ii) approximate these sums by integrals, and (iii) set in Eq. (41) $\gamma_k = \gamma$ for all k (i.e., impose the independence of k). We will discuss and justify these steps below, but before doing that, we investigate the resulting approximation to Eq. (41), given by

$$-\frac{1}{2\pi} \zeta_0^{-2} \int \ln(X_{i,j}/R_0)\, \phi(X_{j,k})\, d^2 r_j + \phi(X_{i,k}) = -\gamma \ln X_{i,k}/R_0, \tag{45}$$

where

$$\zeta_0^{-2} = 2\pi n \left\langle \frac{1}{\ln(R_0/R)} \right\rangle \approx 2\pi n \frac{1}{\ln(R_0/\langle R \rangle)} \tag{46}$$

and the angular brackets denote averaging over the distribution of droplet sizes (that is, the average value obtained in the particular droplet configuration in which $\hat{L}^{-1}$ is evaluated).

The integral equation (45) can be solved easily by operating with ∇_i^2 on the left- and right-hand sides. Using the identity $\nabla^2 \ln r = 2\pi\delta(\vec{r})$, we obtain the following differential equation for $\phi(x)$:

$$-\zeta_0^{-2} \phi + \nabla^2 \phi = -2\pi\gamma\delta(\vec{r}). \tag{47}$$

Its solution is the MacDonald function

$$\phi_{i,k} = \phi(X_{i,k}) = \gamma K_0(X_{i,k}/\zeta_0), \quad i \neq k \tag{48}$$

$$K_0(r/\zeta_0) \approx \begin{cases} -\ln(r/2\zeta_0) - C, & r \ll \zeta_0 \\ \sqrt{\dfrac{\pi\zeta_0}{2r}}\, e^{-r/\zeta_0}, & r \gg \zeta_0, \end{cases} \tag{49}$$

where $C \approx 0.5772$ is Euler's constant.

Let us briefly discuss this result. First of all, note that self-consistency of the approximation imposes positivity of ζ_0^2, i.e., $R_0 \gg \langle R \rangle$. This is indeed the case, as will be discussed below. Next note that the divergence of $\phi(r)$ at short distances is an artifact of the approximations we made by replacing the exact discrete equation (41) by the continuous equation (45). This divergence has no physical consequences since the diagonal elements of the *discrete* matrix $\hat{\phi}$ are not given by taking $r \to 0$ in the solution of Eq. (47); rather, they are determined by Eq. (40). One should note also that if γ_k were to depend on k the result (48) would have become $\phi_{i,k} = \gamma_k K_0(X_{i,k}/\zeta_0)$, implying that $\phi_{i,k} \neq \phi_{k,i}$, whereas the matrices $\hat{T}$ and $\hat{\phi}$ must be symmetric [see Eqs. (36) and (38) and remember that $\hat{L}$ is symmetric].

The diagonal elements are expressed in terms of the off-diagonal ones in Eq. (40); using there the approximations listed above and the mean-field expression (48) for the off-diagonal elements, Eq. (40) becomes

$$\phi_{k,k} \approx \frac{1}{2\pi}\zeta_0^{-2}\int \ln(X_{k,j}/R_0)K_0(X_{j,k}/\zeta_0)d^2r_j = \phi_0\,, \tag{50}$$

as anticipated in Eq. (44). Using this in Eq. (42) yields

$$\gamma_k = 1 + \frac{\phi_0}{\ln(R_k/R_0)}\,,$$

and in order to get a consistent mean-field approach, with γ_k independent of k [as required by assumption (iii)], we must have $\phi_0 = 0$. To set $\phi_0 = 0$ we will now use our freedom to adjust the parameter R_0. As discussed in Sec. II, we are free to vary this parameter since it does not affect the dynamics [24]. Thus we arrive at the following condition on R_0:

$$\phi_0 = \frac{1}{2\pi}\zeta_0^{-2}\int \ln(X_{k,j}/R_0)K_0(X_{j,k}/\zeta_0)d^2r_j = 0. \tag{51}$$

After some simple but lengthy transformations, given in Appendix C, Eq. (51) becomes the following approximate expression for $\ln R_0$:

$$\left\langle \frac{1}{\ln(R_0/R)} \right\rangle \approx \left\langle \frac{1}{K_0(R/\zeta_0)} \right\rangle. \tag{52}$$

Substituting Eq. (52) into Eq. (46) yields a closed equation for ζ_0, with no dependence on R_0:

$$\zeta_0^{-2} = 2\pi n\left\langle \frac{1}{\ln(R_0/R)} \right\rangle \approx 2\pi n\left\langle \frac{1}{K_0(R/\zeta_0)} \right\rangle. \tag{53}$$

Note that once we find ζ_0, we can use this equation also to determine R_0. This will not be necessary since R_0 drops out of the dynamic equations, as shown below. Equation (53) is almost identical to Marqusee's expression for the screening length. In principle we can now proceed as planned; for any droplet configuration evaluate ζ_0, calculate the mean-field approximation to the matrix $\hat{\phi}$,

$$\phi_{i,j} \approx K_0(X_{i,j}/\zeta_0), \quad \phi_{k,k} \approx 0, \tag{54}$$

substitute into Eqs. (38) and (36) to get $\hat{L}^{-1}$, and use it in the dynamics equation (28). There is a problem doing this though. An important property of the *exact* $\hat{L}^{-1}$ is that it satisfies the sum rule (27) and hence the total area of all droplets is conserved by the dynamics [see Eq. (29)]. Since Eq. (54) is an approximation, we have to check the extent to which the sum rules are satisfied by our approximate $\hat{\phi}$. Substituting Eq. (54) into Eq. (36) yields

$$\hat{L}^{-1}_{i,i} = \frac{1}{R_i^2\ln(R_i/R_0)}, \quad \hat{L}^{-1}_{i,j} = \frac{K_0(X_{i,j}/\zeta_0)}{R_i\ln(R_i/R_0)R_j\ln(R_j/R_0)}. \tag{55}$$

Note that $\hat{L}^{-1}_{i,j}$ are small at distances $X_{i,j} \gg \zeta_0$; hence the parameter ζ_0 should be interpreted as a *screening length*. At short distances the solution of Eq. (47) behaves like the lowest-order approximation [i.e., stopping at $n=1$ in the expansion (34)]. Using these expressions in the sum rule (27) gives

$$\sum_j L^{-1}_{i,j}R_j \approx \frac{1}{R_i\ln(R_i/R_0)}\left[1 + \sum_{j\neq i}\frac{1}{\ln(R_j/R_0)}K_0(X_{i,j}/\zeta_0)\right]. \tag{56}$$

When we approximate the sum by an integral, in the spirit of our mean-field approach, it becomes

$$\sum_{j\neq i}\frac{1}{\ln(R_j/R_0)}K_0(X_{i,j}/\zeta_0) \to -\frac{1}{2\pi}\zeta_0^2\int K_0(r/\zeta_0)d^2r = -1$$

and the right-hand side of Eq. (56) vanishes, so that in the mean-field limit (i.e., for vanishing area fraction; see Appendix D) when our approximations become exact, the sum rule is indeed satisfied. If, however, we use Eq. (55) for practical calculations at a nonvanishing area fraction, the sum rule (and hence area conservation) will *not* be satisfied rigorously.

This problem can be overcome rather simply in the following way. Adopt the mean-field approximation (55) for the *off-diagonal* elements of $\hat{L}^{-1}$ and use the sum rule (27) to determine its diagonal elements:

$$\hat{L}^{-1}_{i,i} = -\frac{1}{R_i}\sum_{j\neq i} L^{-1}_{i,j}R_j\,.$$

The result for both diagonal and off-diagonal elements of $\hat{L}^{-1}$ can be summarized as

$$\hat{L}^{-1} = \begin{cases} \dfrac{-1}{R_i^2\ln(R_i/R_0)}\displaystyle\sum_{j(\neq i)}\frac{K_0(X_{i,j}/\zeta_0)}{\ln(R_j/R_0)} & \text{if } i=j \\ \dfrac{K_0(X_{i,j}/\zeta_0)}{R_iR_j\ln(R_i/R_0)\ln(R_j/R_0)} & \text{otherwise.} \end{cases} \tag{57}$$

With this approximation for $\hat{L}^{-1}$ the sum rule is of course exactly satisfied in every step and area is conserved. In the mean-field limit the sum in Eq. (57) yields -1 and the expression for $\hat{L}^{-1}_{i,i}$ obviously reduces to the naive one, given by Eq. (55).

Using Eq. (57) in Eq. (28), we obtain now a rather elegant expression for $\dot{R}_i$, the rates of change of the droplets' radii:

$$\dot{R}_i = \sum_j L^{-1}_{i,j} = \frac{1}{R_i\ln(R_i/R_0)}\sum_{j(\neq i)}\frac{K_0(X_{i,j}/\zeta_0)}{\ln(R_j/R_0)}\left(\frac{1}{R_j} - \frac{1}{R_i}\right). \tag{58}$$

For a given droplet configuration we have now an explicit expression for the dynamics of the droplets' radii (note that the values of the parameters R_0 and ζ_0 are also determined by the configuration). As a final ''cosmetic'' adjustment, we use Eq. (52) to replace logarithms by K_0 (thereby eliminating R_0 from the dynamics), yielding the equation we used in our numerical study:

$$\dot{R}_i = \frac{1}{R_iK_0(R_i/\zeta_0)_j}\sum_{(\neq i)}\frac{K_0(X_{i,j}/\zeta_0)}{K_0(R_j/\zeta_0)}\left(\frac{1}{R_j} - \frac{1}{R_i}\right). \tag{59}$$

To complete the treatment we now justify our naive approach, discuss the regime in which our approximation is expected to hold, and check whether various assumptions

that were made are self-consistent. First of all we assumed that R_0 can be chosen so that $\zeta_0^2>0$. Now we can see from Eq. (52) that the ''optimal'' $R_0\approx\zeta_0$, and since in the mean-field limit $\zeta_0\gg R_i$ this means that $R_0\gg R_i$ for all i, so that by Eq. (46) ζ_0^2 is indeed positive and our approach is self-consistent.

The central point of our approach was replacement of the sum (41) by an integral:

$$\sum_{j\neq i,k}\frac{1}{\ln R_j/R_0}\ln(X_{i,j}/R_0)\phi_{j,k}\rightarrow n\left\langle\frac{1}{\ln R_j/R_0}\right\rangle\int\ln(X_{i,j}/R_0)\phi(X_{j,k})d^2r_j. \tag{60}$$

It is intuitively clear that such a substitution is valid as long as N_ζ, the number of droplets in the screening zone, is large. Now, after having obtained the solution ϕ, we can indeed show that the condition $N_\zeta\gg1$ holds when $\ln(\varphi^{-1})\gg2\pi$ (see Appendix D). Therefore, the conditions for validity of the mean-field result lead to a self-consistent theory only in the limit of very low area fraction $\varphi\rightarrow0$; even for $\varphi\sim0.001$, there are only a few droplets in the screening zone.

For the experimental value $\varphi=0.13$, ζ_0 is about the mean droplet radius, which makes our approximation completely invalid. Such a small value of ζ_0 appears because above we have neglected *all* correlations between the positions of the droplets. In particular it turns out that each of the droplets is surrounded by a *depletion zone*, from which all possible neighbors are excluded (at least the distance between the centers of any two droplets must exceed the sum of their radii). In practice (as seen from our numerical solutions; see below) the mean diameter of the depletion zones d is approximately $2.2\langle R\rangle$. The corrections provided by including the effects of the depletion zones are discussed in Appendix B. As is shown there, taking the depletion zones into account does not change the previously obtained expression for Eq. (16), but the mean field ζ_0 is replaced by a larger screening length ($\zeta_{sc}=2.73\langle R\rangle$ for $\varphi=0.13$), which becomes comparable to the nearest neighbors' distance. Although this improvement is not sufficient to justify our mean-field approach, the numerical results (obtained with the effect of depletion zones taken into account) presented in the next section are in a rather good agreement with the experiments that were performed at $\varphi=0.13$.

IV. THE ALGORITHM AND RESULTS OF THE SIMULATIONS

In this section we describe our numerical procedure and the results of our simulations. Since we would like to reach the scaling state with a sufficiently large number of droplets (to reduce the effect of fluctuations), we must start from initial states with many droplets and allowing this large system to evolve for long times. In order to do this with reasonable computational resources one has to resort to approximations that accelerate the numerical procedure. Rewrite Eq. (59) in the form

$$\frac{dS_\alpha}{dt}=V_\alpha\equiv\sum_\beta v_{\alpha,\beta}, \tag{61}$$

$$v_{\alpha,\beta}=\frac{K_{\alpha,\beta}}{k_\alpha k_\beta}\left(\frac{1}{R_\beta}-\frac{1}{R_\alpha}\right), \tag{62}$$

where we used the abbreviated notation

$$K_{\alpha,\beta}\equiv K_0(X_{\alpha,\beta}/\zeta_{sc}),\quad k_\alpha\equiv K_0(R_\alpha/\zeta_{sc}),\quad S_\alpha\equiv R_\alpha^2/2.$$

The screening length that appears in the argument of the MacDonald functions is $\zeta_{sc}=2.73\overline{R}$, as follows from the analysis of the depletion zones presented in the Appendix B (see Table I at $\varphi=0.13$).

Say we wish to integrate Eqs. (61) and (62) naively. For each time step we have to evaluate all $N(t)$ velocities V_α, with each velocity given by a sum of N terms, i.e., $N_{op}\approx N^2$ operations per time step. If we have initially N droplets and wish to reach the late stages with a few percent surviving, we would have to perform $N_{steps}\sim N$ time steps of integration, as was done by Yao *et al.* [18]. This is so because if the time step is greater than the lifetime of some droplet, its area will become *negative* at the end of the time step, which leads to an increase of the area fraction of the surviving droplets. Therefore, apparently in order to guarantee exact area conservation one must eliminate each shrinking droplet separately, restricting the time step by the next vanishing. At the same time, the detailed evolution of the smallest droplet is absolutely unimportant for us. Rather we would like to choose τ to be not smaller than it is needed to ensure that the relative change of $\langle R\rangle$, the *mean* radius of the droplets, is small during one time step. For this reason, Akaiwa and Meiron [17] simply removed the droplets with $R<\epsilon\langle R\rangle$ with $\epsilon=0.1$ *before* performing the time step. Let f_s be the fraction of the droplets that are eliminated in each time step (it is kept constant, to a good approximation, by fixing ϵ). Then the number of steps needed for a run is reduced to $N_{steps}\approx(1/f_s)\ln N$. However, their procedure still did not guarantee precise area fraction conservation: When the number of droplets was reduced by a factor of 5 (from 100 000 to 20 000), the change of φ was about 2% [18].

We require our algorithm to conserve area fraction *exactly* and nevertheless to reduce both N_{steps} and N_{op}. We achieved $N_{op}\sim N$ and $N_{steps}\sim(1/f_s)\ln N$; that is, our scheme requires $O(N\ln N)$ operations for the entire evolution.

To reduce the N dependence of N_{op} we note that a droplet β, whose separation from α exceeds considerably the screening length, will have only a small contribution to V_α. As will be shown below, only droplets from the *first layer* near α have a significant contribution and therefore only the neighbors of α are included in the sum $V_\alpha=\Sigma_\beta v_{\alpha,\beta}$. Therefore, we have $N_{op}\sim N$ (replacing N^2).

To reduce N_{steps} to $N_{steps}\approx(1/f_s)\ln N$, *conserving the area fraction*, we should treat accurately the vanishing of the small droplets, instead of simply removing them before performing the time step, as is done in Ref. [18]. Putting this into practice requires care however. Let us consider the system of droplets at two consecutive times t_0 and $t_1=t_0+\tau$. We call all droplets that survive to t_1 large and denote them by indices i and j, whereas droplets that vanished before t_1 are called small and are marked by indices n,m. With this notation Eqs. (61) and (62) become

$$\frac{dS_i}{dt}=\sum_j v_{i,j}+\sum_m v_{i,m}, \tag{63}$$

$$\frac{dS_m}{dt}=\sum_n v_{m,n}+\sum_j v_{m,j}. \tag{64}$$

We choose τ to be small enough so that the density of small droplets is small; hence the typical distance between two small droplets exceeds considerably the screening length. Therefore, to an excellent approximation two small droplets do not interact (i.e. $K_{m,n}\approx 0$) and the first term in Eq. (64) can be neglected. Thus Eq. (64) becomes

$$\frac{dS_m}{dt}=\sum_j v_{m,j}=V_m. \tag{65}$$

Then a small droplet will live for time

$$t_m=-S_m/V_m. \tag{66}$$

Turning now to integrate Eq. (63), we note that the term $v_{i,m}$, which represents the contribution of the fast droplet m to the growth of the slow droplet i, is actually present only during the interval t_m and not the entire τ. Hence we must use

$$S_i(t+\tau)=S_i(t)+\left(\sum_j v_{i,j}\right)\tau+\sum_m v_{i,m}t_m,$$

which can be rewritten, using Eq. (66), as

$$S_i(t+\tau)=S_i(t)+\left(\sum_j v_{i,j}+\frac{1}{\tau}\sum_m S_m\frac{v_{i,m}}{V_m}\right)\tau. \tag{67}$$

This is, in fact, the discrete-time form of the differential equation

$$\frac{dS_i}{dt}=\sum_j v_{i,j}+\frac{1}{\tau}\sum_m S_m\frac{v_{m,i}}{V_m}. \tag{68}$$

This equation has a very simple interpretation: The ith large droplet obtains from each of the small droplets a part of the latter's area, proportional to the strength of the interaction between the droplets. Equation (67) is the main working formula of our algorithm. The two terms in the parentheses correspond to (i) redistribution of the material between the large droplets and (ii) absorption of the material that leaves the small droplets onto the large ones. Using Eq. (67) eliminates the fast scale of the dynamics; the time scale τ is to be chosen so that the assumptions made above are indeed satisfied. Our scheme is put to practice by first choosing a convenient *fraction of small droplets*, which is then kept (approximately) *fixed* throughout the run (typically we used $f_s\approx 0.003$, which corresponds to removing ~ 80 droplets at each time step when the system contains 28 000 droplets).

Finally, we should take into account the shift of the droplets. For that one can use either the exact relation

$$\frac{d\vec{r}_i}{dt}=2\sum_{j\neq i}\frac{q_j}{|X_{i,j}|}\frac{\vec{X}_{i,j}}{|X_{i,j}|}, \tag{69}$$

where the charges $q_i=R_i\dot{R}_i$ are evaluated at each time step, or the heuristic formula

$$\frac{d\vec{r}_i}{dt}=2\sum_{j\neq i}\frac{K_{j,i}}{k_ik_j}\left(\frac{1}{R_i}-\frac{1}{R_j}\right)\frac{\vec{X}_{i,j}}{|X_{i,j}|^2}, \tag{70}$$

discussed in the Introduction and Appendix A. Then we proceed according the following steps.

(i) Pick R_s such that the number of droplets with $R_n\leq R_s$ is approximately $N_s=f_sN$. (In practice $R_s/\langle R\rangle$ is kept fixed; in the scaling state this is the same as fixing f_s.) Identify these as small droplets and calculate all V_m using Eq. (64).

(ii) An estimate $\tau^{(0)}$ for the time step is determined as the interval during which all small droplets vanish,

$$\tau^{(0)}=\max_m\{t_m\},$$

where t_m is determined by Eq. (66).

(iii) Calculate the velocities of the large droplets $V_i=\Sigma_j v_{i,j}$ (summing over neighbors of i only; hence this step takes $\sim N$ operations). Note that some droplet i that has been classified as large may in fact disappear during the interval $\tau^{(0)}$; this happens if the velocity is such that $S_i<-V_i\tau^{(0)}$. All such droplets, if any, are collected and reclassified as small, a new value for τ is determined, and the velocities (both V_m and V_i) are recalculated. Usually one such iteration suffices to reach a self-consistent classification.

(iv) Integrate Eq. (68) one step τ, that is, calculate new areas according to Eq. (67).

(v) Calculate the shifts of the droplets according to either Eq. (69) or (70) and repeat the procedure.

Since the relaxation time needed to reach the scaling state depends on how close the initial configuration is to this state, one would like to choose the initial configuration reasonably close to it. We prepared our initial state as follows. We generated a set of $N=50\,000$ droplets with a distribution of radii close to the expected one (determined from short preparatory runs). We scattered them over the plane at random but so that each droplet is surrounded by a small depletion zone (free of other droplets), to mimic the effect of correlations that appear in the real evolving system. For this initial configuration we started a rather large time step τ (and run the dynamics without moving droplets) yielding only an approximation to the true dynamics. This preliminary relaxation went on until the number of droplets was reduced to $N=28\,000$. At this point a smaller time step was selected, the droplets were allowed to move, and we started to take measurements. All the results presented below are averaged over eight runs in order to reduce statistical fluctuations.

In our first simulations we did not take into account the shift of droplets. As is shown in Appendix A, this frozen droplets approximation might be good even for fractions as large as $\varphi=0.13$. In order to test this, we executed runs with frozen droplets and measured the fraction f_c of droplets crossing each other, as a function of the number of droplets in the system. These data are presented in Fig. 1. It shows a considerable growth of f_c with time (from zero at $N=28\,000$ to 10% at $N=1000$) and there is no tendency towards stabilization. This proves that the droplets' motion has

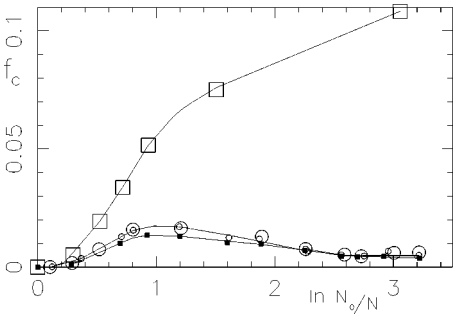

FIG. 1. Time dependence of f_c, the fraction of crossing droplets, as obtained from the frozen droplets model (empty squares); from model B, which uses the heuristic Eq. (70) for the droplets' shift (full squares), and from model A, which uses the exact Eq. (69) for the droplets shift (large circles and small circles for small and large summation block sizes $b=4.1\zeta$ and $b=5.8\zeta$, respectively; see explanations in the text). The lines are guides for the eye. The growth of f_c observed for the frozen droplets model indicates that it is not valid for the area fraction $\varphi=0.13$. On the other hand, once the droplets are allowed to move, f_c decreases to very small values irrespective of whether model B or A is used.

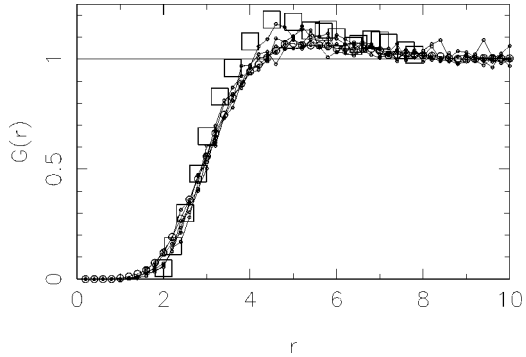

FIG. 2. Correlation functions of droplets' positions $G(r)$ as measured at different moments of time in the scaling state, corresponding to $N=3000$, 2000, 1500, 1300, and 1000 droplets present (small circles). The weighted average of these runs (the weight of a configuration is proportional to the corresponding number of droplets) is also shown (large circles). These results were obtained using model B. Note that all the lines are close to each other, indicating that the system has indeed arrived at the scaling state. The experimental results of Krichevsky and Stavans, shown for comparison (squares), are also close to ours.

a considerable effect on the dynamics of the system and hence the model of frozen droplets is invalid for such large φ.

Taking the droplets' shift into account improves this situation drastically. We used both Eqs. (69) and (70) (called models A and B, respectively; see below) for the droplets' motion. Figure 1 shows that both models A and B give rise to much smaller values of f_c and that it saturates at long times. Interestingly, while there is no essential difference between these two models, the heuristic model B exhibits slightly lower values of f_c than model A. In order to test the convergence of the sum in Eq. (69) we executed runs with different numbers of terms in the sum taken into account, namely, we varied the size of the summation box from $b=4.1\zeta_{sc}$ to $b=5.8\zeta_{sc}$ and found no noticeable difference in the behavior of f. Thus we conclude that we have achieved proper convergence of Eq. (69).

We now present results of our simulations, performed at the same relative area fraction $\varphi=0.13$ that was studied experimentally [3]. We measured the position correlation function $G(r)$, that is, the mean number of the droplets whose centers lie within an annulus $[r,r+dr]$ around the center of a given one. Figure 2 presents $G(r)$ obtained running model B at three consequent moments of time, when the system contained 3000, 2000, and 1000 droplets, respectively (each of the curves is averaged over *eight* runs). We see that the three curves coincide up to their fluctuations, which proves that the scaling state has indeed been reached. The corresponding experimental data are also presented in this figure; good agreement is seen. Figure 3 compares the position correlation functions obtained by the models A and B (averaged over time in the scaling state). This proves that our heuristic formula works perfectly. The experimental $G(r)$ has a noticeable maximum at $r\approx 4.7$, while for our curves the maximum is smaller; at the same time our curve is rather close to the result of Masbaum (see Fig. 1(a) in Ref. [14]), which has a small peak as well, which cannot be distinguished clearly from the fluctuations. Note that in Ref. [14] the data were taken with $N\sim 800$ droplets, whereas our data are well averaged (effectively they correspond to a system of about 50 000 droplets in the scaling state) and the small peak is definitely observed.

Analysis of the distribution of the droplets' radii at three consequent moments of time, where the system contained 3000, 2000, and 1000 droplets, respectively, also shows that the distribution achieved its stationary form. No clear difference between the models A and B was seen. The droplets' radii distribution in the scaling state, averaged over time, as obtained from our simulations (model B), is shown in Fig. 4 together with the experimental results. A certain discrepancy is seen, however, that does not exceed by much the statistical errors of the experimental points.

Finally, we measured the charge correlation functions [3], which contain more detailed information about the system, defined as follows. For a charge q_i calculate $Q_+(r)$, the total amount of similar charge as q_i within an annulus $[r,r+dr]$ around $\vec{r}_i$, and define the function

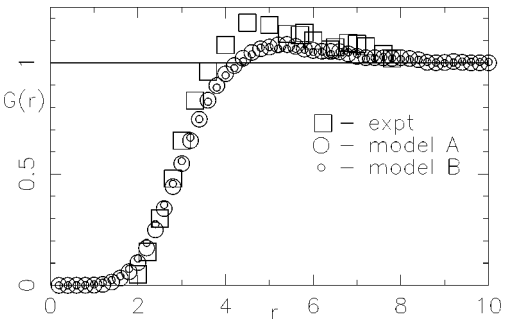

FIG. 3. Weighted time average (the weight of a configuration is proportional to its number of droplets) of the correlation functions of droplets' positions $G(r)$ (averaged over eight runs) for models A and B in the scaling state (large circles and small circles, respectively). The experimental results of Krichevsky and Stavans are also shown (squares). This shows that the two models give indistinguishable results that are in good agreement with experiment as well.

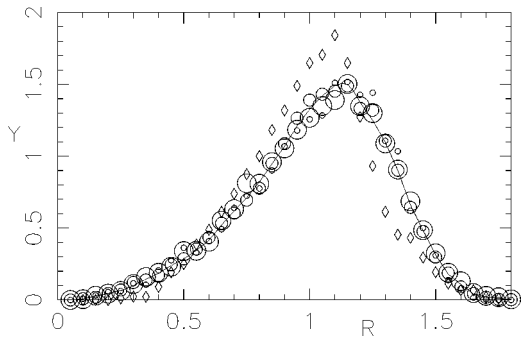

FIG. 4. $Y(R)$, the droplets' rescaled size distribution in the scaling state at $N=3000$ (largest circles), $N=2000$ (intermediate circles) and $N=1000$ (small circles). Each plot presents the average over eight runs. The line indicates the overall average. The experimental results of Krichevsky and Stavans are also shown (diamonds).

$$g_+(r)=\langle q_i Q_+(r)\rangle.$$

Similarly we define $g_-(r)$ in terms of the *opposite* charges. These two functions, as obtained by simulation of the two models, are presented in Fig. 5 together with the corresponding experimental data by Krichevsky and Stavans. The agreement can be characterized as excellent. Again, there is no noticeable difference between the results of models *A* and *B*.

One should notice that our definition of the charge correlation functions $g_\pm(r)$ is not precisely the same as that of Ref. [3]. Krichevsky and Stavans smeared a droplet's charge on its perimeter before calculating $Q_\pm(r)$, whereas we assigned a droplet's charge to its center. We believe, however, that the smearing of the charge on the droplet's perimeter is no more than a way of smoothing the data and there is no essential difference between the two definitions.

V. SUMMARY

Ostwald ripening is the coarsening process, observed during the late stage of the evolution of a two-phase system, where the droplets of the minority phase exchange material by means of diffusion. This process leads towards a scaling state in which the characteristic length scale grows with time according to the scaling law $\widetilde{R}\sim t^{1/3}$, while all the statistical properties (such as the droplets' size distribution, position correlation functions, etc.), once rescaled, remains fixed.

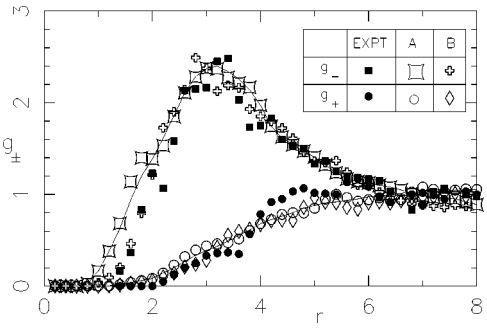

FIG. 5. Charge correlation functions (see precise definition in the text) for the same $[g_+(r)]$ and the opposite $[g_-(r)]$ charges, as obtained using models *A* and *B*, compared with the experimental data of Krichevsky and Stavans (full circles and full squares for the same and the opposite charges, respectively). The lines are guides for the eye. Our data present averages over eight runs. Note that the fluctuations in this plot are larger than for the position correlation function (see Fig. 2). We believe that the difference between the results of the two models is due to the fluctuations. Interestingly, model *B* seems to be closer to the experimental points.

The problem of calculating these characteristics has been studied in a number of detailed numerical simulations that take into account all the complicated interactions between the droplets, mediated by the diffusion field. These calculations, although being exact, do not contribute much to a qualitative understanding of the importance of different components of the interaction between the droplets. On the other hand, analytical mean-field treatments neglect all spatial effects and seem to be oversimplified.

The aim of this paper was to construct and test a ''minimal extension'' of the mean-field approach that will take into account spatial effects, keeping only the simplest interaction between the droplets. We calculated analytically an approximate form of these interactions using a mean-field approach. Only pairwise interactions between the droplets were preserved. We proposed a very efficient numerical algorithm, which allows us to follow the evolution of tens of thousands of droplets. We tested our approach by comparing its results with the experimental data and found surprisingly good agreement at a relatively large value of the minority phase area fraction $\varphi=0.13$, where our approach to the interaction between the droplets was not expected to work.

Trying to find the simplest model that reproduces the experimental data, we examined the importance of a number of effects. Our findings are summarized as follows.

(i) Depletion zones have a considerable effect on the screening length, increasing it from $\zeta=1.88\overline{R}$ to $\zeta=2.73\overline{R}$. At the same time, as shown in Table I, the presence of the depletion zones almost does not affect the functional form of the pairwise interaction between the droplets.

(ii) Our approach is based on the assumption of circular droplets and the monopole plus dipole approximation for the diffusion field. The agreement obtained with the experiment indicates that at the values of φ studied higher multipoles can be neglected.

(iii) Even though inclusion of the depletion zones increases the screening length ζ too little to provide formal validity to our approximation, our simulations show that it works even for $\varphi=0.13$.

(iv) The effect of the droplets' motion is very important for large area fractions, although formally it could be regarded as adiabatically small compared to the droplets growth.

(v) The expression that determines the shift of the droplets requires summation over a large number of droplets. We propose a much simpler heuristic formula (containing a sum over the nearest neighbors only) that gives even better results than the exact one.

An advantage of our method is its computational efficiency; we are able to choose time steps no smaller than required by physical reasonability, eliminating a large number of droplets at each step. At the same time, the total area of the droplets is conserved exactly at each time step. This makes our approach useful for extensive studies of the Ostwald problem.

ACKNOWLEDGMENTS

This research was supported by grants from the Germany-Israel Science Foundation. B. L. thanks the Clore Foundation for financial support. We thank O. Krichevsky, J. Stavans, and D. Kandel for most useful discussions.

APPENDIX A: ANALYSIS OF THE FORMULA FOR THE DROPLETS' SHIFT

The droplets' shifts are determined by Eq. (20):

$$\frac{d\vec{r}_i}{dt}=2\sum_{j\neq i}\frac{q_j}{|X_{i,j}|}\frac{\vec{X}_{i,j}}{|X_{i,j}|}. \tag{A1}$$

First of all, using this formula we can show that in the low area fraction limit the shift of the positions can be neglected. Indeed, τ_{sh}, the characteristic time of a shift of a droplet's center of mass, is given by

$$\tau_{sh}^{-1}\sim\frac{1}{X_{i,j}}\left|\frac{d\vec{X}_{i,j}}{dt}\right|\sim\frac{q_i}{X_{i,j}}. \tag{A2}$$

The characteristic growth time of the droplet is [see Eq. (12)]

$$\tau_{gr}^{-1}\sim\frac{1}{R_i}\left|\frac{d\vec{R}_i}{dt}\right|\sim\frac{q_i}{R_i^2}. \tag{A3}$$

Comparing Eqs. (A2) and (A3) we see that

$$\tau_{sh}^{-1}\sim\tau_{gr}^{-1}\frac{R_i^2}{X_{i,j}^2}=\tau_{gr}^{-1}\frac{\varphi}{\pi}. \tag{A4}$$

That is, for small area fractions the motion of the droplets' centers is adiabatically slower than their growth. Consequently, one can neglect the droplets' motion and the system is characterized only by the dynamics of the droplets' radii as determined by Eqs. (13) and (14). Formally, one can expect this approximation to be valid even for $\varphi=0.13$ (used in the experiments by Stavans and Krichevsky) and we have tried it in our work (see Sec. IV and Fig. 1). Our simulations have shown, however, that neglecting the droplets' motion gives wrong results and therefore the dynamics of the $\vec{r}_i$ has been taken into account.

Secondly, note that a rough estimate of the sum on the right-hand side of Eq. (A1) indicates that it exhibits bad convergence properties. Assuming q_j to be uncorrelated random variables with zero mean we get

$$\left\langle\left(\frac{d\vec{r}_i}{dt}\right)^2\right\rangle\sim\langle q^2\rangle\sum\frac{1}{|X_{i,j}|^2}\sim\langle q^2\rangle\ln L_s, \tag{A5}$$

where L_s is the size of the system. A more accurate treatment implies, however, that the sum does converge. According to Eqs. (12)–(16)

$$q_j=R_j\frac{dR_j}{dt}=\sum_{m\,(\neq j)}K_{j,m}\Delta_{j,m},$$

where

$$\Delta_{j,m}=\frac{1}{k_m k_j}\left(\frac{1}{R_m}-\frac{1}{R_j}\right)$$

and we use the abbreviations $K_{j,i}=K_0(X_{j,i}/\zeta_{sc})$ and $k_j=K_0(R_j/\zeta_{sc})$. Then Eq. (A1) becomes

$$\frac{1}{2}\frac{d\vec{X}_i}{dt}=\sum_{j\,(\neq i)}Q_j^{(i)}\frac{\vec{X}_{i,j}}{|X_{i,j}|^2}+\sum_{j\,(\neq i)}\sum_{m\,(\neq j,i)}Q_j^{(m)}\frac{\vec{X}_{i,j}}{|X_{i,j}|^2}, \tag{A6}$$

where

$$Q_i^{(j)}\equiv K_{j,i}\Delta_{j,i}$$

denotes the part of the charge on the ith droplet that is induced by the jth one. The first term of Eq. (A6) determines the shift of the droplet due to the direct material transferred between this droplet and its jth neighbors. This sum converges very well because $Q_i^{(j)}$ decreases exponentially with distance $X_{i,j}$. The second term accounts for the effect of the redistribution of the material between the jth and mth droplets. Since the internal sum (on m) contains a short-range factor $K_{j,m}$, it is actually over a $\zeta\times\zeta$ box around the jth droplet. In this double sum, each term

$$Q_j^{(m)}\frac{\vec{X}_{i,j}}{|X_{i,j}|^2}$$

can be paired with

$$Q_m^{(j)}\frac{\vec{X}_{i,m}}{|X_{i,m}|^2}.$$

Since $Q_j^{(m)}=-Q_m^{(j)}$, these two contributions can be considered as a *dipole*. Thus each $\zeta\times\zeta$ box represents a dipole $\vec{P}$ (randomly directed) with the dipole moment $P\sim q\zeta$, where q is the characteristic scale of $Q_m^{(j)}$. Thus the second term in Eq. (A6) is now estimated as

$$\begin{aligned}(\text{second term})&\sim\sum_{\zeta\times\zeta\text{ boxes}}\frac{\vec{P}}{|X_{i,j}|^2}-\frac{2(\vec{P}\cdot\vec{X}_{i,j})\vec{X}_{i,j}}{|X_{i,j}|^4}\\&\sim\sum\frac{\vec{P}}{|X_{i,j}|^2}.\end{aligned} \tag{A7}$$

The mean of this expression is zero, while the mean square deviation is given by

$$\sim q^2\zeta^2\sum\frac{1}{|X_{i,j}|^4}, \tag{A8}$$

which converges to a finite value. Thus, when calculating the sum in Eq. (A1), we can restrict ourselves to only several nearest layers of neighbors.

Finally, one can use an even simpler heuristic formula for calculating the shift of the droplets. The meaning of Eq. (A6) is that the motion of ith droplet has two sources. The first is the material transferred between this droplet and its jth neighbors [the first term of Eq. (A6)]. The second is due to

redistribution of the material between the surrounding jth droplets themselves (the second term). Although these contributions are of the same order, in our case we have a reason to drop the second term (although it does not simplify computations, it does makes the model physically simpler). The shift of the droplets has a noticeable effect only at relatively large fractions, where the interaction between the next nearest neighbors is considerably suppressed. Then, for a fixed configuration of the nearest neighbors of the ith droplet we can vary the configuration of its next nearest neighbors. This manipulation will not affect the first term of Eq. (A6), while it will reduce its second term. Thus, in the mean-field spirit of our model, we can average the shift velocity of the ith droplets over various configurations of its next nearest neighbors. Thus we finally get

$$\frac{d\vec{X}_i}{dt}=2\sum_{j\neq i}\frac{K_{j,i}}{k_i k_j}\left(\frac{1}{R_i}-\frac{1}{R_j}\right)\frac{\vec{X}_{i,j}}{|X_{i,j}|^2}. \tag{A9}$$

Although the approximation leading to this formula is not based on a rigorous expansion, our simulations show that it works as well as the more rigorous equation (A1). At the same time it is much more economic because it requires the summation only over the nearest neighbors.

APPENDIX B: DEPLETION ZONES

The simplest possible improvement over the mean-field approximation can be obtained by including some of the correlations between the positions of the droplets' centers. In this appendix we will take into account the simplest manifestation of these correlations: the so called *depletion zones*. These are the regions around each of the droplets, from which all possible neighbors are excluded (by geometrical steric constraints, the distance between the centers of any two droplets must exceed at least the sum of their radii).

The *exact* equation for the diagonal elements of the matrix $\hat{\phi}$ is given by Eq. (41), whereas for the off-diagonal elements it is Eq. (39):

$$\sum_{j\neq i,k}\frac{1}{\ln R_j/R_0}\ln(X_{i,j}/R_0)\,\phi_{j,k}+\phi_{i,k}=-\gamma_k\ln X_{i,k}/R_0. \tag{B1}$$

This has been replaced in our mean-field approximation by the following integral equation for the smooth function $\phi(x)$ [see Eq. (45)]:

$$-\frac{1}{2\pi}\zeta_0^{-2}\int\ln(X_{i,j}/R_0)\,\phi(X_{j,k})\,d^2r_j+\phi(X_{i,k})=-\gamma\ln X_{i,k}/R_0. \tag{B2}$$

Clearly, by using the integral of Eq. (B2), we implicitly assume that the distribution of $\vec{r}_j$, the positions of the centers of droplets j, are independent of their distance from the one at $\vec{r}_i$. This homogeneity assumption may serve as a reasonable approximation as long as $\overline{X}$, the mean distance between neighbors, is much greater than d, the typical radius of the depletion zones. However, when the density increases to the extent that $\overline{X}\sim d$, the inhomogeneity of the distribution of the j droplets around the fixed droplets i and k can no longer be ignored. One should emphasize that other effects, such as correlations between different charges and between the droplets' sizes, may also be of importance and can also possibly affect the elements of the inverse matrix we are calculating. Nevertheless, here we take into account only the correlations that ensure that the areas of two neighbors do not overlap. In our actual numerical calculations even this is done only approximately, by introducing a *uniform* sized depletion zone, neglecting its fluctuations as well as dependence on the droplets' radii.

Correlation between the positions of the droplets can be incorporated in our approximate treatment by replacing the sum in Eq. (B1) by the integral operator

$$\hat{S}_{int}\phi=-\frac{1}{2\pi}\zeta_0^{-2}\int\ln(X_{i,j}/R_0)P(\vec{r}_i,\vec{r}_j,\vec{r}_k)\,\phi(X_{j,k})\,d^2r_j, \tag{B3}$$

where P is the probability of finding a droplet centered at the point $\vec{r}=\vec{r}_j$, given that there are droplets at $\vec{r}=\vec{r}_i$ and $\vec{r}=\vec{r}_k$. We approximate this probability (three-point correlation function) by representing it as the product of pair-correlation functions

$$P(\vec{r}_i,\vec{r}_j,\vec{r}_k)=g(X_{i,j})g(X_{j,k}), \tag{B4}$$

where $g(X_{i,j})$ is the probability of finding a droplet j at distance $X_{i,j}$ from the center of droplet i; this function is normalized such that $g(r)\to 1$ at $r\to\infty$. Within this approximation Eq. (B1) is replaced by

$$\hat{S}_{int}\phi+\phi(X_{i,k})=-\left(1+\frac{\phi_{k,k}}{\ln(R_k/R_0)}\right)\ln X_{i,k}/R_0 \tag{B5}$$

where now we have

$$\hat{S}_{int}\phi=-\frac{1}{2\pi}\zeta_0^{-2}\int\ln(X_{i,j}/R_0)g(X_{i,j})g(X_{j,k})\,\phi(X_{j,k})\,d^2r_j. \tag{B6}$$

In order to solve Eq. (B5) we first try to bring it as close to the form of Eq. (B2) as we can and then use the same method of solution as was used there. To this end we first rewrite the expression for $\hat{S}_{int}$ as

$$\hat{S}_{int}\phi=-\frac{1}{2\pi}\zeta_0^{-2}\int\ln(X_{i,j}/R_0)g(X_{i,j})\,\phi(X_{j,k})\,d^2r_j+\frac{1}{2\pi}\zeta_0^{-2}\int\ln(X_{i,j}/R_0)g(X_{i,j})\times[1-g(X_{j,k})]\,\phi(X_{j,k})\,d^2r_j. \tag{B7}$$

The pair-correlation function $g(X)$ vanishes for short distances $X<d$ and $g\approx 1$ for large X. Therefore, we get nonvanishing contributions to the second term in Eq. (B7) only when $X_{j,k}<d$. For $X_{i,k}\gg d$, we have in this region $g(X_{i,j})\approx 1$ and $\ln(X_{i,j}/R_0)\approx\ln(X_{i,k}/R_0)$, so that

$$\hat{S}_{int}\phi \approx -\frac{1}{2\pi}\zeta_0^{-2}\int \ln(X_{i,j}/R_0)g(X_{i,j})\phi(X_{j,k})d^2r_j - \frac{1}{2\pi}\zeta_0^{-2}\ln(X_{i,k}/R_0)\int [1-g(X_{j,k})]\phi(X_{j,k})d^2r_j . \tag{B8}$$

The last formal step we take is to express the first integral here as the sum of two terms, using $-g=[1-g]-1$, which leads to our final expression for $\hat{S}_{int}\phi$:

$$\hat{S}_{int}\phi = -\frac{1}{2\pi}\zeta_0^{-2}\int \ln(X_{i,j}/R_0)\phi(X_{j,k})d^2r_j + \frac{1}{2\pi}\zeta_0^{-2}\int \ln(X_{i,j}/R_0)[1-g(X_{i,j})]\phi(X_{j,k})d^2r_j - \frac{1}{2\pi}\zeta_0^{-2}\ln(X_{i,k}/R_0)\int [1-g(X_{j,k})]\phi(X_{j,k})d^2r_j . \tag{B9}$$

Our basic equation (B5) takes now the form

$$-\frac{1}{2\pi}\zeta_0^{-2}\int \ln(X_{i,j}/R_0)\phi(X_{j,k})d^2r_j+\phi(X_{i,k}) + \frac{1}{2\pi}\zeta_0^{-2}\int F(X_{i,j})\phi(X_{j,k})d^2r_j=-\gamma_k\ln(X_{i,k}/R_0), \tag{B10}$$

where

$$\gamma_k=1+\frac{\phi_{k,k}}{\ln(R_0/R_k)}+\frac{1}{2\pi}\zeta_0^{-2}\int [1-g(X_{j,k})]\phi(X_{j,k})d^2r_j \tag{B11}$$

and

$$F(X)=\ln(X/R_0)[1-g(X)]. \tag{B12}$$

Note that Eq. (B10) is very close in form to Eq. (B2); the only significant difference is the appearance of a new term, the integral over the function F, which contains explicitly the correlation function g. Clearly, when $g(X)\equiv 1$ we recover Eq. (B2). As was the case there, the solution of Eq. (B10) is symmetric if and only if γ_k does not depend on k, $\gamma_k\approx\gamma$, which is achieved by imposing $\phi_{k,k}=0$. This leads again to a condition that determines the value of the parameter R_0 [see Eq. (B21) below]. Although now $\gamma\neq 1$ [see Eq. (B11)], its value is unimportant for the simulations since it can be absorbed in the definition of the time scale in the dynamic equation. Hence, below we will set $\gamma=1$.

We solve Eq. (B10) by first applying the ∇_i^2 operator to the equation, which yields

$$-\zeta_0^{-2}\phi(X_{i,k})+\nabla_i^2\phi(X_{i,k}) + \frac{1}{2\pi}\zeta_0^{-2}\nabla_i^2\int F(X_{i,j})\phi(X_{j,k})d^2r_j=-2\pi\gamma\delta(X_{i,k}). \tag{B13}$$

Denote the Fourier transform of $F(X)$ by

$$\tilde{F}(q)=\frac{1}{2\pi}\int d^2r\ln\left(\frac{r}{R_0}\right)[1-g(r)]e^{i\vec{q}\cdot\vec{r}} = \int_0^\infty r\, dr\ln\left(\frac{r}{R_0}\right)[1-g(r)]J_0(qr). \tag{B14}$$

Note that the integral converges, since $g(r)\to 0$ fast for large r. Upon Fourier transforming Eq. (B13) becomes

$$-\zeta_0^{-2}\tilde{\phi}(q)-q^2\tilde{\phi}(q)-\zeta_0^{-2}q^2\tilde{F}(q)\tilde{\phi}(q)=-2\pi\gamma, \tag{B15}$$

yielding the solution for $\tilde{\phi}(q)$ (from now on we set $\gamma=1$)

$$\tilde{\phi}(q)=\frac{2\pi}{q^2}\,\frac{1}{1+\zeta_0^{-2}[\tilde{F}(q)+q^{-2}]}. \tag{B16}$$

Once $\tilde{\phi}(q)$ has been evaluated, the function $\phi(X)$ is obtained by the inverse Fourier transform. From this point on we work with the specific (step-function) form of $g(X)$:

$$g(X)=\begin{cases}0, & X<d\\ 1, & X>d.\end{cases} \tag{B17}$$

For this form of g the integral in Eq. (B14) can be calculated analytically, integrating by parts and using the identities $[xJ_1(x)]'=xJ_0(x)$ and $[J_0(x)]'=J_1(x)$ to get

$$\tilde{F}(q)=q^{-2}\{-q\,dJ_1(qd)\ln(R_0/d)+[1-J_0(qd)]\}. \tag{B18}$$

We now substitute this into (B16) and perform the angular integration in the inverse Fourier transform to arrive at the following expression for $\phi(r)$:

$$\phi(r)=\int_0^\infty \frac{J_0(qr)}{q^2+\zeta_0^{-2}-[\zeta_0^{-2}\ln(R_0/d)]q\,dJ_1(qd)+\zeta_0^{-2}[1-J_0(qd)]}q\;dq. \tag{B19}$$

We cannot perform this integral analytically, but it is simple to evaluate by numerical integration. Once this has been done, the parameter R_0 can be found by imposing the condition $\phi_{k,k}=0$, which takes the form [analogous to Eq. (51)]

$$\phi_{k,k}=\frac{1}{2\pi}\zeta_0^{-2}\int \ln\left(\frac{r}{R_0}\right)g(r)\phi(r)d^2r=0, \tag{B20}$$

which becomes the following equation for R_0:

$$\ln R_0=\frac{\int_d^\infty \ln(r)\phi(r)r\;dr}{\int_d^\infty \phi(r)r\;dr}. \tag{B21}$$

Once R_0 has been determined, we can evaluate the parameter ζ_0, using its definition

$$\zeta_0^{-2}=2\pi n\left\langle\frac{1}{\ln(R_0/R_i)}\right\rangle. \tag{B22}$$

For a given droplet configuration one can now proceed to find $\phi(r)$ by taking the following steps. First, determine the radius of the depletion zone d from the measured correlation function of the droplets (such as Fig. 3). Then solve Eqs. (B19), (B21), and (B22). This can be done iteratively by initializing the procedure using the results of the correlation-free theory for ϕ, ζ_0, and R_0. The next iterate of $\phi(r)$ is evaluated using Eq. (B19). This new $\phi(r)$ is then used in Eq. (B21) to yield the new value of R_0. This in turn is used in Eq. (B22), together with the distribution of the droplets' radii, to yield the new iterate of ζ_0. The procedure is then repeated until convergence is reached. In practice we used a few simplifying steps, which made computation faster without significantly altering the result. The first simplification consists of setting

$$d=\kappa\langle R\rangle \tag{B23}$$

for an entire run, instead of determining it from the correlation function at each time step. We found that values in the range $2.0\leqslant\kappa\leqslant 2.8$ fit the correlation function quite well. The numerical results were obtained using the fixed value $\kappa=2.15$. A second time-saving simplification is to use the approximation

$$\zeta_0^{-2}=2\pi n\frac{1}{\ln(R_0/\langle R\rangle)} \tag{B24}$$

to calculate ζ_0, instead of evaluating the average $\langle 1/\ln(R_0/R_i)\rangle$ over the measured distribution of droplet sizes. Recall also that the density of droplets n is related to their relative area fraction φ by $n=\varphi/\pi\langle R^2\rangle$. In the spirit of the previous approximation we replace $\langle R^2\rangle\approx\langle R\rangle^2$, so that Eq. (B24) becomes

$$\zeta_0^{-2}=\frac{2\varphi}{\langle R\rangle^2}\frac{1}{\ln(R_0/\langle R\rangle)}. \tag{B25}$$

Using Eqs. (B23) and (B25) simplifies our numerical scheme significantly. To demonstrate the effect of including the depletion zones in the calculation we present in Table I the results of calculations performed in the scaling regime at four different values of φ. The various quantities presented were obtained as follows: R_0 and ζ_0 are (simultaneous) solutions of Eqs. (B19), (B21) (with $d=2.15\langle R\rangle$ in both), and (B25). ζ_0^{mf} is the value of the screening length as obtained by setting $d=0$. The screening length ζ_{scr} is the first moment of the function $\phi(r)$,

$$\zeta_{scr}^2=\int_d^\infty \phi(r)r\;dr, \tag{B26}$$

calculated by numerical integration of Eq. (B19).

As we see, for very small fractions the screening length is less than ζ_0^{mf}. This is surprising since we expected inclusion of the depletion zones to increase the screening regions. For the larger fractions, however, we indeed see that the effect of including the depletion zone changes sign: The renormalized screening length becomes greater than the mean-field result, as was expected.

Another important observation we should make is that as φ increases, ζ decreases and becomes comparable to the average radius (in units of which it is given in Table I). At such φ, ζ obviously cannot be interpreted as a ''screening length'' because $\zeta\approx\langle R\rangle$ means that there are no droplets in the ''screening zone.''

Another question that we studied in detail concerns the extent to which introducing the depletion zone affects the function $\phi(r)$. Clearly, when we are not in the limit of very small φ it is no longer given by the MacDonald function. Table II contains $\phi(r)$, as obtained at $\varphi=0.13$ by the procedure outlined above: setting $d=2.15\langle R\rangle$ and simultaneously solving Eqs. (B19), (B21), and (B25). Comparing $\phi(r)$ with the simple mean-field result $K_0(r/\zeta_0^{mf})$ reveals that the renormalization due to inclusion of the depletion zones leads to a significant change of the matrix elements $\phi(r)$. On the other hand, comparing $\phi(r)$ with the function $K_0(r/\zeta_0)$ we see that $\phi(r)$ does not differ much from MacDonald's function, provided the *renormalized* ζ_0 is used. Therefore, in principle this function can be used in calculations as a fairly good approximation for $\phi(r)$. The numerical results presented in Sec. IV were obtained using $\zeta_0=2.73$, according to Table I.

APPENDIX C: DERIVATION OF THE CONDITION FOR R_0

The condition (45) on R_0:

$$\frac{1}{2\pi}\zeta_0^{-2}\int \ln(X_{k,j}/R_0)K_0(X_{j,k}/\zeta_0)d^2r_j=0, \tag{C1}$$

TABLE II. Interaction function $\phi(r)$ for the case of depletion zones calculated at the area fraction $\varphi=0.13$. It is compared with the MacDonald function with the renormalized screening parameter ζ_0 (third column) and with the unrenormalized, mean-field screening length ζ_0^{mf} (fourth column). Note that the distance r is measured in units of the mean distance between neighboring droplets $x=1/\sqrt{n}$.

r/x	$\phi(r)$	$K_0(r/\zeta_0)$	$K_0(r/\zeta_{mf})$
0.722	2.884	2.617	1.205
0.884	1.914	1.773	0.711
1.045	1.320	1.218	0.425
1.206	0.901	0.845	0.257
1.420	0.546	0.525	0.133
1.689	0.297	0.294	0.059
1.904	0.185	0.186	0.031
2.012	0.147	0.148	0.022
2.118	0.118	0.118	0.016
2.333	0.075	0.076	0.008
2.548	0.046	0.048	0.004
2.763	0.027	0.031	0.002
2.97	0.016	0.020	0.001
3.031	0.014	0.018	0.001
3.353	0.0087	0.0095	0.00047

can be simplified by representing

$$\ln(X_{i,j}/R_0)=\ln(X_{i,j}/\zeta_0)+\ln(\zeta_0/R_0)$$

so that Eq. (C1) becomes

$$B+A\ln(\zeta_0/R_0)=0\,, \tag{C2}$$

where the constant A has the value

$$A=\frac{1}{2\pi}\zeta_0^{-2}\int K_0(X_{j,k}/\zeta_0)d^2r_j=1 \tag{C3}$$

because of the normalization of $K_0(x)$, while the other constant B is given by

$$B=\frac{1}{2\pi}\zeta_0^{-2}\int \ln(X_{k,j}/\zeta_0)K_0(X_{j,k}/\zeta_0)d^2r_j\,. \tag{C4}$$

In order to evaluate B we note that the solution of Eq. (45) is given, for any value of R_0, by Eq. (48). Therefore, we can substitute $\phi(X_{i,k})$ from Eq. (48) in Eq. (45) and choose for R_0 the special value $R_0=\zeta_0$ to get the identity

$$-\frac{1}{2\pi}\zeta_0^{-2}\int \ln(|\vec{r}-\vec{r}'|/\zeta_0)K_0(r'/\zeta_0)d^2r'+K_0(r/\zeta_0)$$
$$=-\ln(r/\zeta_0)\,. \tag{C5}$$

It is trivial to see that in the limit $\vec{r}\to 0$ the integral on the left-hand side of this identity becomes precisely equal to B [as given by Eq. (C4)]. For $\vec{r}\to 0$ we can use the small-r limit (49) of K_0 so that for very small r our identity becomes

$$-B-\ln\left(\frac{r}{2\zeta_0}\right)-C=-\ln\left(\frac{r}{\zeta_0}\right),$$

so that we find

$$B=\ln 2-C \tag{C6}$$

(C is Euler's constant). Using the values of A and B in Eq. (C2) it becomes

$$\ln 2-C+\ln(\zeta_0/R_0)=0\,, \tag{C7}$$

providing a new connection between R_0 and ζ_0. This is to be used together with Eq. (46) to solve for both R_0 and ζ_0. Since Eq. (46) contains $\ln(R_0/\langle R\rangle)$, it is convenient to add and subtract $\ln\langle R\rangle$ from Eq. (C7) and to rewrite it as

$$\ln(R_0/\langle R\rangle)=\ln(2\zeta_0/\langle R\rangle)-C. \tag{C8}$$

If we have $\langle R\rangle\ll\zeta_0$ the right-hand side of Eq. (C8) is $\approx K_0(\langle R\rangle/\zeta_0)$, so that Eq. (C7) becomes $\ln(R_0/\langle R\rangle)\approx K_0(\langle R\rangle/\zeta_0)$. Finally, we can write, with the same accuracy,

$$\left\langle\frac{1}{\ln(R_0/R)}\right\rangle\approx\left\langle\frac{1}{K_0(R/\zeta_0)}\right\rangle. \tag{C9}$$

APPENDIX D: THE SMALL PARAMETER OF THE APPROXIMATION

In the mean-field limit, when $R_0\sim\zeta_0\gg R_i$ the quantity $1/\ln(R_0/R_i)$ does not vary much and one can take it out of the sum and replace it by its mean value. Next we see that there is a scale ζ_0 such that ϕ does not change much over distances much less than ζ_0. Let us divide the plane into boxes b of size $\zeta_0\times\zeta_0$. Then the sum that still remains can be rewritten as

$$\sum_{j\neq i,k}\ln(X_{i,j}/R_0)\phi_{j,k}=\sum_b\sum_{j\in b\ (j\neq i,k)}\ln(X_{i,j}/R_0)\phi_{j,k}\,. \tag{D1}$$

Actually, only the few boxes located near $\vec{r}_k$ have a significant contribution to the sum; the contribution of all the others is exponentially small due to the screening effect.

The expression being summed does not change much inside each box and therefore, if the mean number of the droplets in the box N_ζ is large enough, the internal sum within each box can be replaced by the integral. In this case, according to the theorem of large numbers,

$$\left|\sum_{j\in b}\ln(X_{i,j}/R_0)\phi_{j,k}-n\int\ln(X_{i,j}/R_0)\phi(X_{j,k})d^2r_j\right|\sim\frac{1}{\sqrt{N_\zeta}}. \tag{D2}$$

This gives rise to the following condition for the validity of our approximation:

$$N_\zeta=n\zeta_0^2\gg 1. \tag{D3}$$

However, Eq. (46) implies that $n\zeta_0^2 \sim (2\pi)^{-1}\ln(R_0/\langle R\rangle)$ and, as we have shown, $\zeta_0 \approx R_0$, so that

$$n\zeta_0^2 \sim \ln(\zeta_0/\langle R\rangle). \tag{D4}$$

On the other hand, multiplying Eq. (46) by $\langle R\rangle^2$ and using the definition of the area fraction $\varphi = \pi n\langle R^2\rangle \sim \pi n\langle R\rangle^2$ yields $\ln(\zeta_0/R_0) \sim \ln(\varphi^{-1})$. This, together with Eqs. (D3) and (D4), means that

$$\ln(\varphi^{-1}) \gg 2\pi.$$

[1] D. Gunton, M. San Miguel, and P. Sahni, in *Phase Transitions and Critical Phenomena*, edited by C. Domb and J. L. Lebowitz (Academic, London, 1983), Vol. 8, p. 267, and references therein.

[2] W. Ostwald, Z. Phys. Chem. **34**, 495 (1900).

[3] O. Krichevsky and J. Stavans, Phys. Rev. Lett. **70**, 1473 (1993); Phys. Rev. E **52**, 1818 (1995).

[4] E. M. Lifshitz and L. P. Pitaevskii, *Physical Kinetics* (Pergamon, Oxford, 1982), p. 432.

[5] E. M. Lifshitz and V. V. Slyozov, J. Phys. Chem. Solids **19**, 35 (1961).

[6] C. Wagner, Z. Elektrochem. **65**, 581 (1961).

[7] J. A. Marqusee, J. Chem. Phys. **81**, 976 (1984).

[8] J. H. Yao, K. R. Elder, H. Guo, and M. Grant, Physica A **204**, 770 (1994).

[9] M. Marder, Phys. Rev. A **36**, 858 (1987).

[10] Q. Zheng and J. D. Gunton, Phys. Rev. A **39**, 4848 (1989).

[11] J. W. Cahn and J. E. Hilliard, J. Chem. Phys. **28**, 258 (1989).

[12] A. Chakrabarti, R. Toral, and J. D. Gunton, Phys. Rev. E **47**, 3025 (1993).

[13] T. M. Rogers and R. C. Desai, Phys. Rev. B **39**, 11 956 (1989).

[14] N. Masbaum, J. Phys. I **5**, 1143 (1995).

[15] T. Imaeda and K. Kawasaki, Physica A **164**, 335 (1990).

[16] N. Akaiwa and P. W. Voorhees, Phys. Rev. E **49**, 3860 (1994).

[17] N. Akaiwa and D. I. Meiron, Phys. Rev. E **51**, 5408 (1995); Phys. Rev. E **54**, 13 (1996).

[18] J. H. Yao, K. R. Elder, H. Guo, and M. Grant, Phys. Rev. B **47**, 14 110 (1993).

[19] C. W. J. Beenakker, Phys. Rev. A **33**, 4482 (1986).

[20] M. Marder, Phys. Rev. Lett. **55**, 2953 (1985).

[21] J. A. Marqusee and J. Ross, J. Chem. Phys. **80**, 536 (1984).

[22] C. W. J. Beenakker and J. Ross, J. Chem. Phys. **83**, 4710 (1985).

[23] When fluctuations in R_j are neglected, this equals $1/\ln(\langle R\rangle/R_0)$.

[24] The role of the parameter R_0 in our theory is analogous to the parameter Δ in Beenakker's model [19]; while being irrelevant for the exact problem, it was tuned in order to restore conservation of material, broken in the reduced description.